http://dx.doi.org/10.21577/0100-4042.20170733 *Quim. Nova,* Vol. 44, No. 7, 824-829, 2021

Artigo

SALICYLIC ACID INCORPORATION IN Fe_3O_4-BSA NANOPARTICLES FOR DRUG RELEASE

Renata P. Neves[a,b], Erika S. Bronze-Uhle[c], Pâmela L. Santos[d], Paulo N. Lisboa-Filho[e] and Aroldo G. Magdalena[a,*].
[a]Departamento de Química, Faculdade de Ciências, Universidade do Estado de São Paulo, 17033-360 Bauru – SP, Brasil
[b]School of Sciences - University of Ottawa, Ottawa, Ontario, Canada
[c]Departamento de Dentística, Endodontia e Materiais odontológicos, Faculdade de Odontologia, Universidade de São Paulo, 17012-901 Bauru – SP, Brasil
[d]Departamento de Ciências da Saúde, Universidade de Araraquara, 14801-340 Araraquara – SP, Brasil
[e]Departamento de Física, Faculdade de Ciências, Universidade do Estado de São Paulo, 17033-360 Bauru – SP, Brasil

Recebido em 22/01/2021; aceito em 23/02/2021; publicado na web em 12/03/2021

The controlled release of Salicylic Acid (SA) influences the concentration and collateral effects of the drug. This release refers to the matrix in which the SA is incorporated. Among the matrices, Fe_3O_4 nanoparticles (NPs) stand out, for transporting drugs to specific sites. The functionalization of Fe_3O_4 by bovine serum albumin (BSA) can improve colloidal and chemical stability, in addition to increasing interactions with drugs. Thus, understanding the release kinetics of the AS incorporated in Fe_3O_4-BSA is essential to improve the controlled release. The study aimed the synthesis, characterization and release of the SA into the Fe_3O_4-BSA NPs. The results showed the functionalization of the Fe_3O_4-BSA NPs was effective and the average size was below 30 nm. The NPs showed colloidal stability above the pH of 7.5 which can be used as a drug carrier in blood plasma. Drug encapsulation into the NPs system was efficient (~91%) with about 30% of drug loading capability. The kinetic results showed the SA release mechanism was controlled by diffusion. The conclusion is that the incorporation of SA in Fe_3O_4-BSA NPs led to a release of SA in the first six hours, reaching equilibrium at 0.265 mg mL^{-1} and 1.83 mg.

Keywords: iron oxide; nanoparticles; functionalization; drug delivery.

INTRODUCTION

Nanoparticles has advanced rapidly and it is currently the object of study of many researchers due to the possibilities presented. In the medical field, multifunctional nanoparticles combine multiple therapeutic functions, such as remotely-controlled and targeted drug delivery, imaging capabilities, and hyperthermia.[1,2] Thus, drug intake, half-life, and dispersion may be enhanced and the side effects and lower dosage of these drugs may be minimized.[3]

Iron oxide (Fe_3O_4) NPs have superparamagnetic properties responsible for the hyperthermia function, as well as high chemical stability, low toxicity, and favorable biocompatibility and biodegradability.[1,4,5] The characteristics for a nanoparticle to have a superparamegnetic behavior is related to the critical size of the nanoparticles, which must be around 10 to 20 nm, and therefore each nanoparticle must have a single magnetic domain.[6] Other characteristic is the blocking temperature, that is associated by the temperature below which thermal fluctuations are stabilized.[7] For a nanoparticle to exhibit superparamagnetic behavior, its temperature must be below the blocking temperature,[6,7] and present the critical size of the nanoparticles within the aforementioned range. According to Wahajuddin and Sumit Arora,[3] Fe_3O_4 NPs present no negative effect in the body, such as thrombosis and blood blockage, because they do not tend to agglomerate. These characteristics corroborate the production of a suitable material for biological magnetic applications such as drug delivery.[8]

Although iron oxide nanoparticles present various advantages, coating these NPs is essential.[3] In this study, Fe_3O_4 nanoparticles are coated with bovine serum albumin (BSA), which has high binding ability, prevents surface oxidation, can increase the blood circulation of nanoparticles, and has lower toxicity.[3,4,9] Albumin works as an active target, meaning it can interact with overexpressed receptors found at the cellular target site, resulting in better and specific drug intake by the cells.[3] The advantages of drug-controlled delivery systems are related to a reduction in the quantity and concentration of drugs and a greater ability to reach the target, minimizing side effects.[10] Regarding the advantages of a release system controlled by magnetic NPs, they are mainly related to the magnetic properties and the ability of these nanoparticles to absorb infrared radiation, microwaves, and ultrasound,[10] in addition to the already proven biocompatibility of iron oxides.[10]

Albumin is one of the most abundant proteins in blood plasma, representing 52% to 62% of the total plasma proteins.[9] The main physiological function of albumin is to maintain blood osmotic pressure and pH and play an important role in transporting a variety of endogenous and exogenous compounds, including fatty acids, metals, amino acids, steroids, and, in some cases, therapeutic drugs.[11] Transport systems based on albumin nanoparticles represent an important strategy, considering that significant amounts of drugs can be incorporated into the particle depending on the different binding sites of albumin.[12] Studies indicate that albumin can be considerably tolerated without any serious side effects and because it has a high binding capacity, significant amounts of drugs can be encapsulated.[12] It is known that albumin is an ideal material for nanoparticle systems with applications in drug delivery.[12]

Salicylic acid (SA) has been used in the treatment and prevention of cancer, type 2 diabetes, and arthritis,[9,13,14] which is beyond the most known and common uses as anti-inflammatory, antifungal, and antibacterial non-steroidal drug.[9,13] The SA is an extremely relevant medication worldwide but it suffers a 50% decomposition when administered orally.[9] Considering this issue and the previously described benefits associated with iron oxide NPs and albumin, Fe_3O_4-BSA-SA nanoparticles were synthesized and characterized. Iron oxide nanoparticles were obtained through the co-precipitation

*e-mail: aroldo.magdalena@unesp.br

method and all samples were analyzed using Fourier transform infrared spectroscopy (FTIR), zeta potential, X-ray diffraction (XRD), fluorescence spectroscopy, and transmission electron microscopy (TEM). Understanding the release kinetics of the AS incorporated in Fe_3O_4-BSA is essential to improve the controlled release. The study aimed the synthesize and characterize Fe_3O_4-BSA nanoparticles, incorporate SA into the nanoparticulate matrix, and study its release.

EXPERIMENT

Materials

Ammonium hydroxide was purchased from Dinâmica (Indaiatuba/São Paulo, Brazil). Bovine serum albumin (BSA) (lyophilized powder, 66 kDa), 8% (v/v) aqueous glutaraldehyde, and salicylic acid were purchased from Sigma-Aldrich (San Luis/Missouri, USA). Absolute ethanol, ferric chloride hexahydrate ($FeCl_3 \cdot 6H_2O$), and ferrous sulfate heptahydrate ($FeSO_4 \cdot 7H_2O$) were obtained from Synth (Diadema/São Paulo, Brazil). All aqueous solutions were prepared with ultra-pure water. All the chemicals used were of analytical grade and without any further purification.

Synthesis of Fe_3O_4 NPs

Fe_3O_4 NPs were prepared by the co-precipitation method in the nitrogen atmosphere, as previously reported,[1,15,16] with some modifications. The $FeCl_3 \cdot 6H_2O$ and $FeSO_4 \cdot 7H_2O$ (molar ratio of 2:1) were added to 200 mL of distilled water with constant magnetic stirring at room temperature. After complete dissolution, the inlet of nitrogen gas began, which minimizes iron oxidation by removing oxygen during the synthesis. After 10 minutes, the pH of the solution was abruptly adjusted with the addition of 20 mL of ammonium hydroxide, and the solution was heated to 45 (±5) °C. The reaction was kept at 45 (±5) °C in the nitrogen atmosphere under constant stirring for 1 hour. The nanoparticles were washed with distilled water repeatedly, up to a pH of 7, and once with ethanol, and then dried in a water bath at 60 °C.

Synthesis of Fe_3O_4-BSA NPs

An amount of 50 mg of Fe_3O_4 NPs in 3 mL of Milli-Q water was added to BSA (200 mg) previously dissolved in 2 mL of Milli-Q water and stirred mechanically (500 rpm) at room temperature (25°C) for 10 minutes. The protein coated the NPs by adding 600 µL of ethanol (added drop by drop) and then 120 µL of 8% (v/v) aqueous glutaraldehyde to cross-link the BSA.[9] The reaction was kept under constant mechanical stirring for 2 hours. The NPs were separated with a magnet and washed three times to remove glutaraldehyde, ethanol, and unreacted BSA. For each purification step, NPs were redispersed in Milli-Q water and lastly in ethanol. The final product was dried in a water bath (40°C), resulting in a nanosized powder.

Synthesis of Fe_3O_4-BSA-SA NPs

The reaction between SA and iron III generates a purple-red complex and this reaction is one of the most used for the identification of SA.[17,18] Thus, for the incorporation of SA the matrix we are proposing was necessary to perform a previous coating with albumin to prevent the interaction of the AS with the Fe_3O_4 nanoparticles.

For the introduction of SA, a double albumin coating was required due to an unwanted interaction between salicylic acid and iron oxide; in this case, Fe_3O_4-BSA NPs were used instead of Fe_3O_4 NPs. An amount of 200 mg BSA was dissolved in 2 mL of Milli-Q water. Then, 20 mg of SA was added and the solution was stirred mechanically (500 rpm) at room temperature for 10 minutes for BSA-SA interaction. The solution received 50 mg of Fe_3O_4-BSA NPs in 3 mL of Milli-Q water. After another 10 minutes, ethanol and glutaraldehyde were added as described in the method for Fe_3O_4-BSA synthesis.[9]

Evaluation of SA release kinetics

The SA release kinetics were evaluated in 10% phosphate-buffered saline (PBS) at room temperature. Then, 12 mg of Fe_3O_4-BSA-SA NPs were added to 7 mL of PBS, which was constantly and mechanically stirred. At predetermined time intervals, 0.5 mL of the release medium was collected and replaced with an equal volume of fresh PBS to preserve the conditions.[9,19] The samples were taken from the supernatant and SA concentration was determined by fluorescence spectroscopy.[9]

The data obtained in the drug release study were adjusted to different kinetic models of drug release. The kinetic models studied were zero-order (equation (1)), first-order (equation (2)), Higuchi (equation (3)), Korsmeyer-Pepas (equation (4)), and Hixson-Crowell (equation (5)).[16,20]

$$Q_t = Q_0 - k_0 t \quad (1)$$

$$\ln Q_t = \ln Q_0 - k_1 t \quad (2)$$

$$Q_t = K_H t^{1/2} \quad (3)$$

$$\frac{Q_t}{Q_\infty} = k_k t^n \quad (4)$$

$$Q_0^{1/3} - Q_t^{1/3} = k_{HC} t \quad (5)$$

where Q_t is the amount of SA released in time t and Q_o is the amount of SA in time zero, t is time and k is the constant of velocity of the models studied. For the Korsmeyer-Peppas model, $Q_t/Q\infty$ corresponds to the amount of SA released and n is associated with the mechanism of SA release.[20] The fitting of the data into the model was assessed by determining plot linearity from the regression factor (R^2).[20]

Drug loading (DL) and Encapsulation efficiency (EE)

The drug loading ratio (DL%) was calculated using equation (6).[19,21] The drug in nanoparticles is the weight of the encapsulated SA, while the weight of nanoparticles is the total weight of the Fe_3O_4-BSA-SA nanoparticles.

$$DL\ (\%) = \frac{\text{Weight of SA in nanoparticles}}{\text{Weight of nanoparticles}} \times 100 \quad (6)$$

The encapsulation efficiency (EE%) was determined using equation (7).[19,21] The weight of the initial drug corresponds to the amount of SA used in the nanoparticle functionalization.

$$EE\ (\%) = \frac{\text{Weight of SA in nanoparticles}}{\text{Weight of initial SA}} \times 100 \quad (7)$$

These two parameters are relevant to determine the effectiveness of the system for drug delivery.

Characterization techniques

Transmission Electron Microscopy (TEM)

The samples were characterized with a Philips CM-200 instrument with a super twin a-lens. The nanoparticles were dispersed in isopropyl alcohol and kept in an ultrasonic bath for 10 minutes.

A drop of the colloidal suspension was inserted into the copper grid covered with a carbon film. The system was allowed to dry before the analysis.

X-ray diffractometer (XRD)

X-ray diffractometer patterns were obtained from a Rigaku-Rint 2000 diffractometer with CuKα radiation (λ = 1.5418 Å). The measurements were performed at the 2θ interval from 10 to 80°, at a scanning speed of 0.04° min^{-1}.

Infrared Spectroscopy (FTIR)

The spectra in the mid-infrared region were obtained using a Vertex 70 spectrometer (Bruker Instruments) through the attenuated total reflectance method and a scanning range between 4000-400 cm^{-1} using diamond crystals.

Zeta potential

The Zetasizer Nano ZS system (Malvern Instruments) was used to measure the zeta potential. The pH variations were controlled using 0.1 mol·L^{-1} HCl or NaOH in 0.001 mol·L^{-1} NaCl solution with support electrolyte.

Fluorescence spectroscopy

Fluorescence spectroscopy allows the presence of SA and BSA to be determined in the nanoparticles. Solutions of 0.05 mg·mL^{-1} of NPs were analyzed with excitation of 280 nm and emission from 310 to 450 nm. This characterization method was also used to obtain and keep track of SA concentration in the release studies: the supernatant samples were analyzed with the settings adjusted to 330 nm for excitation and 405 nm for emission. To determine SA concentration in the samples, a calibration curve was plotted using known concentrations of SA in water and their fluorescence intensity at 405 nm. The spectra were obtained using a microplate spectrofluorometer (Synergy H1 Hybrid reader - BioTek) and a 96-well plate. All measurements were executed in triplicate.

RESULTS AND DISCUSSION

Figure 1 shows the X-ray diffractograms of BSA, SA, and the following nanoparticles: Fe_3O_4, Fe_3O_4-BSA, and Fe_3O_4-BSA-SA. It is possible to verify the characteristic magnetite diffraction peaks in all nanoparticles studied.

Magdalena *et al.*,[22] studied the synthesis of Fe_3O_4 nanoparticles under different conditions and the results show that synthesis in an oxygen-rich environment leads to an oxidation reaction of Fe_3O_4. The results in Figure 1 show that the synthesis of Fe_3O_4 NPs was completely oxidation-inhibited due to the inert condition used. The samples submitted through functionalization with BSA and incorporation of salicylic acid show peaks of α-Fe_2O_3, indicating that part of the surface of the nanoparticles was oxidized. This result was expected as both of these processes were not performed in an inert atmosphere to avoid changes in the incorporation of SA.

Figure 2 shows the TEM images of Fe_3O_4 (Figure 2-a and Figure 2-b) and Fe_3O_4-BSA (Figures 2-c and 2-d) NPs, which presents nanostructures with variety size and shape. The average size of the nanoparticles was 14.7 ± 4.1 nm for Fe_3O_4 NPS and 19.6 ± 5.3 nm for Fe_3O_4-BSA NPS, as shown in the histogram in Figure 3. The average size of the NPS showed a statistically significant difference (P = <0.001).

Figure 2(c) and Figure 2(d) show a layer around the cluster of Fe_3O_4 nanoparticles. This layer is the BSA functionalized. A large peak around 2θ equals to 20° in Figure 1 for the Fe_3O_4-BSA and Fe_3O_4-BSA-SA, which is a characteristic of albumin. The verification

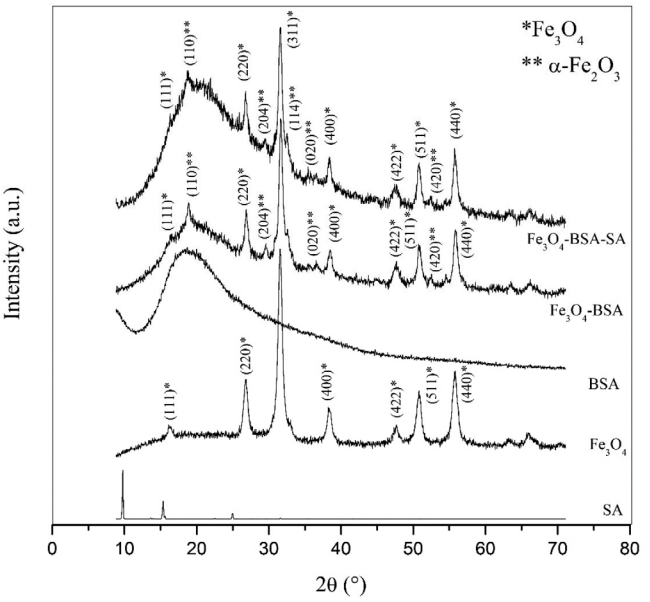

Figure 1. *X-ray diffraction patterns for the samples. The crystalline planes observed in the diffractograms refer to magnetite (Fe_3O_4) (Crysmet n°. 867299) and to hematite (α-Fe_2O_3) (Crysmet n°. 854228)*

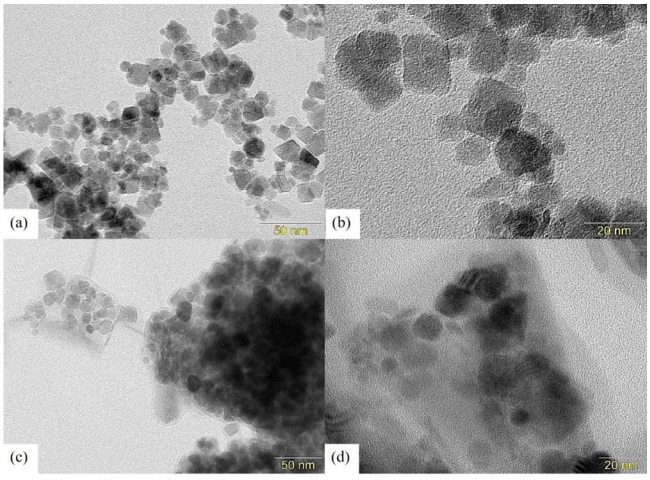

Figure 2. *TEM images of (a) and (b) Fe_3O_4 and (c) and (d) Fe_3O_4-BSA NPs*

of this peak (Figure 1) along with microscopic (Figure 2-c and Figure 2-d) observation show that albumin is functionalizing and that protein coating was efficient.

The synthesized NPs, NPs after the release study, pure BSA, and SA were analyzed and their infrared spectra are shown in Figure 4. The characteristic iron oxide absorption peak between 537 and 670 cm^{-1}, which corresponds to the Fe-O bonding, is present in the FTIR spectra of all synthesized nanoparticles. For the coated NPs, this absorption band shifted towards 551 cm^{-1} and it is less intense due to BSA functionalization on the surface of the magnetic nanoparticles. Additionally, another layer of BSA and SA incorporation shifted these bands to 556 cm^{-1}, and even for the Fe_3O_4-BSA-SA NPs after 10 hours of SA release, this band is observed around 543 cm^{-1}. Therefore, iron oxide is present in all BSA-coated nanoparticles, even after hours of drug release. The small peak at 1625 cm^{-1} relates to water absorption, while the large peak at 3300 cm^{-1} is associated with the ν (O-H) stretch, which proves there are hydroxyl groups on the surface of the iron oxide NPs.[22]

It is possible to identify new peaks in the spectra of the coated nanoparticles in comparison to pure Fe_3O_4. These are attributed to surface modification with albumin.[4] The characteristic absorption

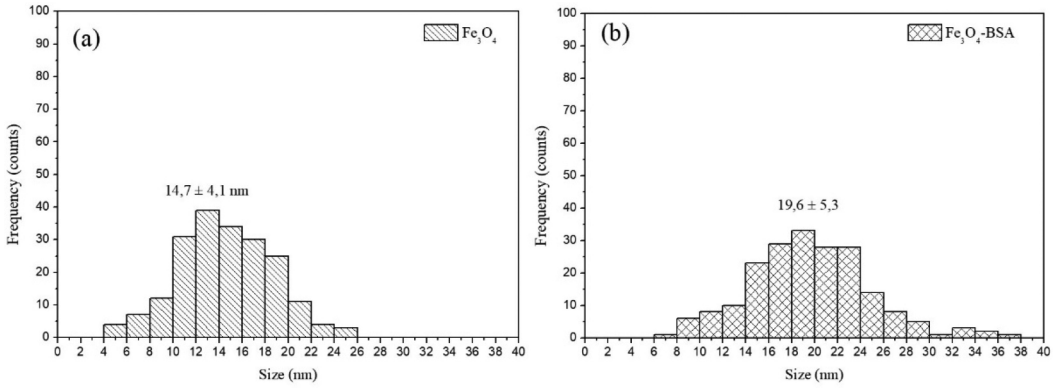

Figure 3. *Histogram obtained for nanoparticles (a) Fe_3O_4 and (b) Fe_3O_4-BSA*

peaks of BSA occur at 3280 cm^{-1} (amide A: N-H stretch), 2978 cm^{-1} (amide B: N-H stretch of free NH_3^+ ions), 1642 cm^{-1} (amide I: C=O stretch), 1520 cm^{-1} (amide II: N-H flexural vibrations and C-N stretch), and 1390 cm^{-1} (CH_2 bending groups).[9,15,23] As presented by Figure 4, the typical absorption peaks of BSA could be found in the spectra of all coated NPs, including the sample taken after drug release. The FTIR analysis indicates that BSA coating was successful and hours of drug release did not remove all the BSA functionalized on the Fe_3O_4 surface.

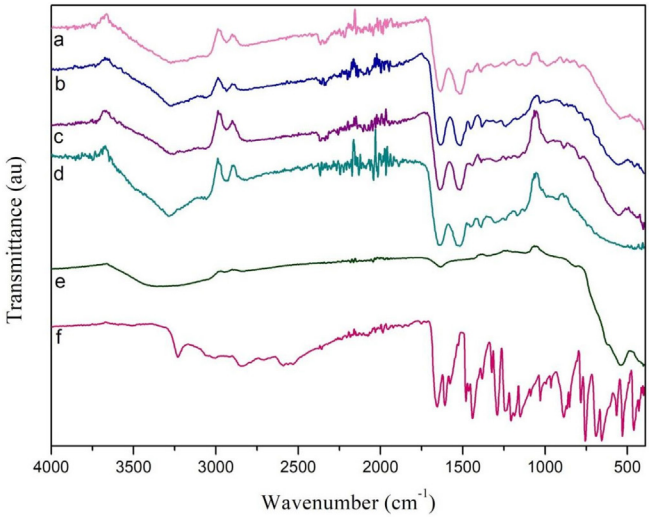

Figure 4. *FTIR spectra. Sample after 10 h of drug release (a), Fe_3O_4-BSA-SA (b), Fe_3O_4-BSA (c), BSA (d), Fe_3O_4 (e), and SA (f)*

Table 1 shows the most relevant wavenumber observed in Figure 4. The A, B, and I amide peaks shifted slightly in comparison to pure BSA, suggesting an interaction between BSA and iron oxide.[15] However, the characteristic amide II band at 1520 cm^{-1} did not shift, therefore no observable interaction took place on this site of the molecule.

It was not possible to identify the characteristic salicylic acid bands in the FTIR spectra because many BSA bands are found in the same region and the concentration of SA in Fe_3O_4-BSA-SA NPs is small in comparison to BSA. However, the shift of the characteristic amide I absorption band is also related to the interaction with salicylic acid, as shown in Table 1.

Figure 5 shows the zeta potential curves as a function of pH for Fe_3O_4 and Fe_3O_4-BSA NPs. It can be verified that the isoelectric point of pure magnetite is slightly higher than that of BSA-functionalized nanoparticles. Bovine serum albumin is an amphiphilic protein due to the presence of the -NH_2 and -COOH groups in its molecular structure. These results corroborate those obtained in the FTIR curves (Figure 4) showing that a chemical interaction occurs between the magnetic nanoparticles and BSA.

According to Han-Wei *et al.*,[24] the best pH value for good

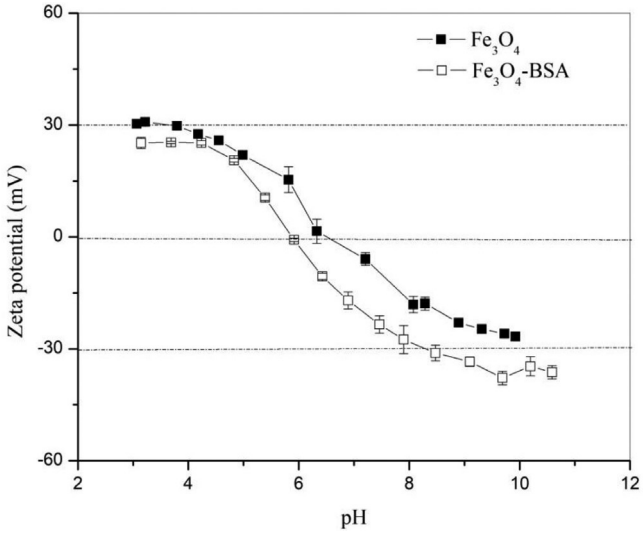

Figure 5. *Zeta potential measurements as a function of pH: Fe_3O_4 and Fe_3O_4-BSA nanoparticles*

Table 1. Main absorption wavenumbers of the FTIR spectra

Attribution	SA (cm^{-1})	BSA (cm^{-1})	Fe_3O_4 (cm^{-1})	Fe_3O_4-BSA (cm^{-1})	Fe_3O_4-BSA-SA (cm^{-1})	After 10 h of SA release (cm^{-1})
Amide A	-	3280	-	3262	3273	3275
Amide B	-	2978	-	2975	2984	2984
Amide I	-	1642	-	1639	1633	1637
Amide II	-	1520	-	1520	1520	1520
CH_2 bending groups	-	1390	-	1387	1383	1388
Fe-O	-	-	537	551	556	543

biocompatibility with blood plasma is in the 7.4-8.0 range. Therefore, the pH of the suspension of BSA-coated Fe_3O_4 nanoparticles should be controlled to be within this range and remain constant. The data obtained in this analysis shows that the zeta potential has a discrete variation above the pH of 7.5. These results indicate that this system has good conditions to work as a carrier in a biological environment.

According to Bronze-Uhle *et al.*,[9] it is possible to analyze the intrinsic fluorescence of BSA and SA at emission wavelengths of 335 and 405 nm, respectively, when the samples are excited at 280 nm. Figure 6 presents the fluorescence spectra of the nanoparticles in this study.

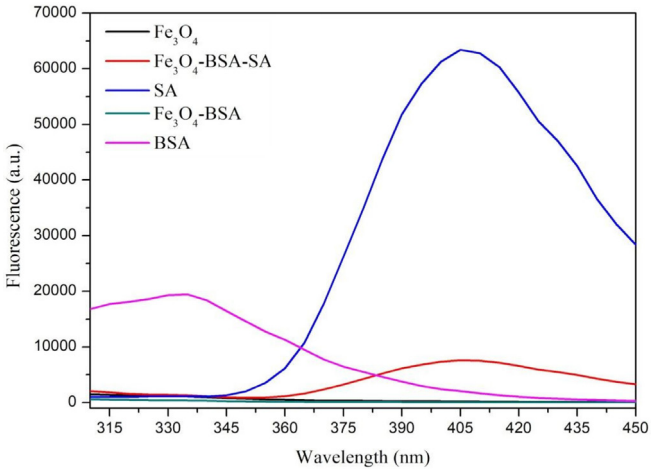

Figure 6. *Fluorescence spectra of the nanoparticles studied*

Coating the NPs with BSA led to a decrease in intensity at 335 nm, which indicates a change in protein conformation as a result of crosslinking and interactions with iron oxide and glutaraldehyde.[9] The peak at 405 nm, which is a characteristic emission of SA, could only be found in the fluorescence spectrum of the Fe_3O_4-BSA-SA NPs. The decreased intensity, compared to pure SA, is due to its low concentration and interactions with BSA in the NPs. The fluorescence wavelength changes indicate conformational and chemical changes in Fe_3O_4, Fe_3O_4-BSA, and Fe_3O_4-BSA-SA NPs, and confirm the salicylic acid encapsulation process.

The release of SA in PBS was analyzed by fluorescence spectroscopy and the results are shown in Figure 7. Most salicylic acid is released in the first six hours and after this time, the cumulative concentration and mass reaches the release balance of about 0.265 mg mL^{-1} and 1.83 mg of the SA, respectively, which is associated with approximately 50% of SA release. This result is promising because it is a slower release than that obtained by Bronze-Uhle *et al.*,[9] in a system of BSA-SA nanoparticles, leading to the conclusion that the presence of magnetite and changes in the procedure were effective to obtain a different drug release profile.

As mentioned previously, the efficiency of drug incorporation and drug loading was calculated. About 91% of salicylic acid used in the synthesis was encapsulated by the nanoparticles and the drug loading was approximately 30%. The increase in the efficiency of the Fe_3O_4-BSA-SA system against BSA-SA,[9] is due to the presence of Fe_3O_4 nanoparticles. The results of SA release are similar to the results obtained by Marudova *et al.*,[25] with blends of chitosan and poly (lactic acid).

The release mechanism of salicylic acid was analyzed using the kinetic models of zero-order, first-order, Higuchi, Korsmeyer-Peppas, and Hixson-Crowell.[20,26]

The results of the coefficient of determination (R^2) of the adjustments to the experimental data are shown in Table 2. Based on the results, the best fit was the Korsmeyer-Peppas model with (R^2 = 0.863) and n = 0.197. The n coefficient is associated with the drug release mechanism. The n values of Korsmeyer-Peppas are mostly lower than 0.5, suggesting the release mechanism was controlled by diffusion.[27] This result is in accordance with Sozer *et al.*,[28] and Several works reported the diffusional process, its release kinetics being studied by the Korsmeyer-Peppas equation.[28-32]

The diffusional mechanism depends on some important parameters such as the thickness, hydrophilicity of the polymeric matrix and the solubility of the drug in the polymeric matrix. The drug molecules can dissolve in the polymer with the formation of covalent bonds or they can be dispersed in the polymeric matrix.[30,33] According to Lopes *et al.*,[34] only dissolved drugs contribute to the diffusion process. In addition, the diffusion process may be occurring alone or as part of the mechanism, as verified by Abbasnezhad *et al.*,[30] According to Bronze-Ulhe *et al.*,[9] the AS interacts in BSA sites I and II, mainly with the groups Tyrosine (Tyr), Tryptophan (Trp) and

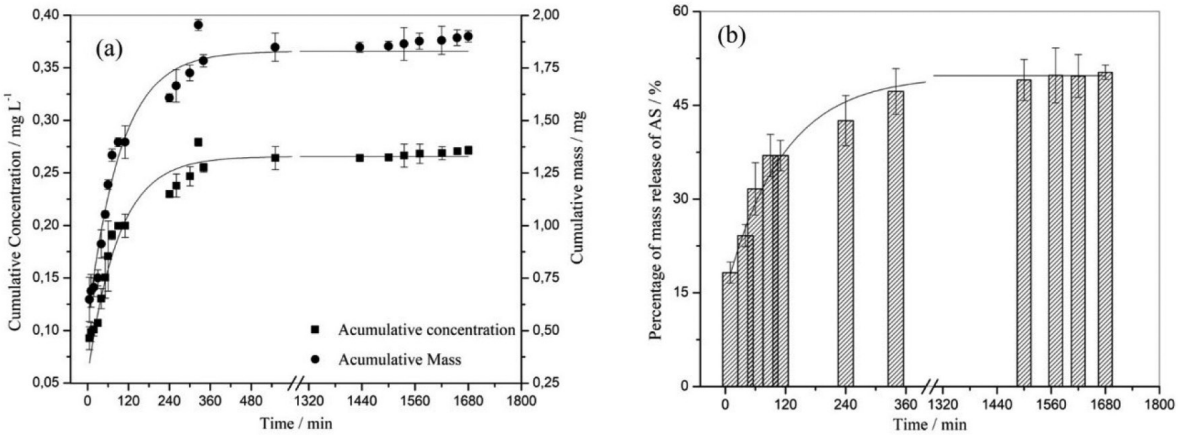

Figure 7. *(a) Cumulative concentration and mass of SA corresponds to the total time of drug release in PBS. (b) Percentage of mass release as function on time*

Table 2. Kinetic models for the release of salicylic acid

	Zero-order	First-order	Higuchi	Korsmeyer-Peppas		Hixson-Crowell
	R^2	R^2	R^2	R^2	n	R^2
Fe_3O_4-BSA-AS	0.524	0.577	0.455	0.863	0.197	0.560

phenylalanine (Phe), thus SA has a certain solubility in BSA which makes the process diffusive mechanism is a plausible mechanism for its release. The presence of Fe_3O_4 nanoparticles does not seem to alter the SA release mechanism, but it did slow their release compared to the BSA-AS system.[9,28]

CONCLUSIONS

The results showed that Fe_3O_4-BSA-SA nanoparticles were successfully synthesized with high encapsulation efficiency (~91%) and the release results are promising. The size of the nanoparticles was 14.7 ± 4.1 nm for Fe_3O_4 NPS and 19.6 ± 5.3 for Fe_3O_4-BSA. The system developed showed colloidal stability above the pH of 7.5, indicating that this material can be used as a drug carrier in blood plasma. The 30% drug loading obtained gives margin to work on the amount of SA desired for each application. Most of the encapsulated SA is released in the first six hours, reaching equilibrium at 0.265 mg mL^{-1} and 1.83 mg of the SA (approximately 50% of SA release), which is well above the results described in BSA-SA studies. The kinetic results showed that the mechanism of SA release was controlled by diffusion.

ACKNOWLEDGMENTS

The authors would like to thank Professor Chibuike Udenegwe of the University of Ottawa for reading and making suggestions for the article.

The authors would like to thank the São Paulo Research Foundation (FAPESP) grant No. 2017/25523-7 and acknowledge CEPID/CDMF – (FAPESP) grant No. 2013/07296-2.

REFERENCES

1. Hao, H.; Ma, Q.; He, F.; Yao, P.; *J. Mater. Chem. B* **2014**, *2*, 7978.
2. Shalviri, A.; Chan, H. K.; Raval, G.; Abdekhodaie, M. J.; Liu, Q.; Heerklotz, H.; Wu, X. Y.; *Colloids Surf., B* **2013**, *101*, 405.
3. Wahajuddin, A. S.; *Int. J. Nanomed.* **2012**, *7*, 3445.
4. Iwaki, Y.; Kawasaki, H.; Arakawa, R.; *Anal. Sci*. **2012**, *28*, 893.
5. Hu, P.; Yu, L.; Zuo, A.; Guo, C.; Yuan, F.; *J. Phys. Chem. C **2009**, 113*, 900.
6. Lu, A-H.; Salabas, E. L.; Scüth, F.; *Angew. Chem., Int. Ed*. **2007**, *46*, 1222.
7. Guimarães, A. P.; *Rev. Bras. Ens. Fis.* **2000**, *22*, 382.
8. Kinsella, J. M.; Ananda, S.; Grondek, J. F.; Chien, M-P.; Scadeng, M.; Gianneschi, N.; Ruoslahti, E.; Sailor, M.; *Adv. Mater*. **2011**, *23*, H248.
9. Bronze-Uhle, E. S.; Costa, B. C.; Ximenes, V. F.; Lisboa-Filho. P. N.; *Nanotechnol. Sci. Appl.* **2017**, *10*, 11.
10. Arruebo, M.; Fernandez-Pacheco, R.; Ibarra, M. R.; Santamaría, J.; *Nano Today* **2007**, *2*, 22.
11. Brandes, N.; Welzel, P. B.; Werner, C.; Kroh, L. W.; *J. Colloid Interface Sci.* **2006**, *299*, 56.
12. Irache, J. M.; Merodio, M.; Arnedo, A.; Camapanero, M. A.; Mirhahi, M.; Espuelas, S.; *Mini Rev. Med. Chem.* **2005**, *5*, 293.
13. Demirdirek, B.; Uhrich, K. E.; *Int. J. Pharm.* **2017**, *528*, 406.
14. Mojtabataghizadeh, S.; Javan, S. R. S.; *e-Polymers* **2010**, *10*, 036.
15. Li, Z.; Quiang, L.; Zhong, S.; Wang, H.; Cui, X.; *Colloids Surf., A* **2013**, *436*, 1145.
16. Nosrati, M.; salehiabar, M.; Manjili, H. K.; Danafar, H.; Davaran, *S.; Int. J. Biol. Macromol*. **2018**, *108*, 909.
17. Oliveira, C. A. F.; Resende-Filho, J. B. M.; Andrade, L. R. *QNEsc* **2011**, *33*, 125.
18. Luz, L. T. S.; Gomes, S. I. A. A; Sandri, M. C. M.; Mello, F.; Bolzan, J. A. *Educ. Quim.* **2019**, *30*, 54.
19. Salehiabar, M.; Nosrati, H.; Javani, E.; Aliakbarzadeh, F.; Manjiili, H. K.; Davaran, S.; Danafar, H.; *Int. J. Biol. Macromol*. **2018**, *115*, 83.
20. Muthappa, R.; Purushothaman, B. K.; Begun, K. M. M. S.; Maheswari, P. U.; *Chem. Prod. Process Model.* **2020**, 20190026.
21. Davidov-Pardo, G.; Joye, I. J.; Mcclements, D. J.; *Adv. Protein Chem. Str*. **2015**, *98*, 293.
22. Magdalena, A. G.; Silva, I. M. B.; Marques, R. F. C.; Pipi, A. R. F.; Lisboa-Filho, P. N.; Jafelicci Jr., M.; *J. Phys. Chem. Solids* **2018**, *113*, 5.
23. Mosrati, H.; Sefifi, N.; Sharafim A.; S.; Danafar, H.; Manjiili, H. K.; *Bioorg. Chem*. **2018**, *76*, 501.
24. He, H. W.; Liu, H. J.; Zhou, K. C.; Wang, W.; Rong P. F.; *J. Cent. South Univ. Technol.* **2006**, *13*, 6.
25. Marudova, M.; Yorov, T.; *Int. J. Polym Mater.* **2019**, *68*, 1.
26. Basak, S. C.; Kumar, K. S.; Ramalingam, M.; *Braz. J. Pharm*. **2008**, *44*, 477.
27. Permanadewi, I.; Kumoro, D. H.; Wardhani, D. H.; Aryanti, N. *J. Phys. Conf. Ser*. **2018**, *1295*, 012063.
28. Sozer, S. C.; Egesoy, T. O.; Basol, M.; Akdogan, G. C.; Akadogan, Y.; *J. Drug Deliv. Sci. Techonol.* **2020**, *60*, 101931.
29. Alinavaz, S.; Mahdavinia, G. R.; Jafari, H.; Hazrati, M.; Akbari, A.; *J. Mol. Struct.* **2021**, *1225*, 129095.
30. Abbasnezhad, N.; Zirak, N.; Shirinbayan, M.; Kouidri, S.; Salahinejad, E.; Tcharkhtchi, A.; Bakir, F.; *J. Appl. Polym. Sci.* **2021**, *138*, 50083.
31. Aycan, D.; Yayla, A. N.; Aydim, Y. A.; *Polym. Degrad. Stab.* **2020**, *181*, 109346.
32. Rahim, M.; Mas Haris, M. R. H.; *Mater. Today Chem.* **2021**, *19*, 100401.
33. Siepmann, J.; Siepmann, F.; *J. Control. Release* **2012**, *161*, 351.
34. Lopes, C. M.; Lobo, J. M. S.; Costa, P.; *Braz. J. Pharm. Sci.* **2005**, *41*, 143.